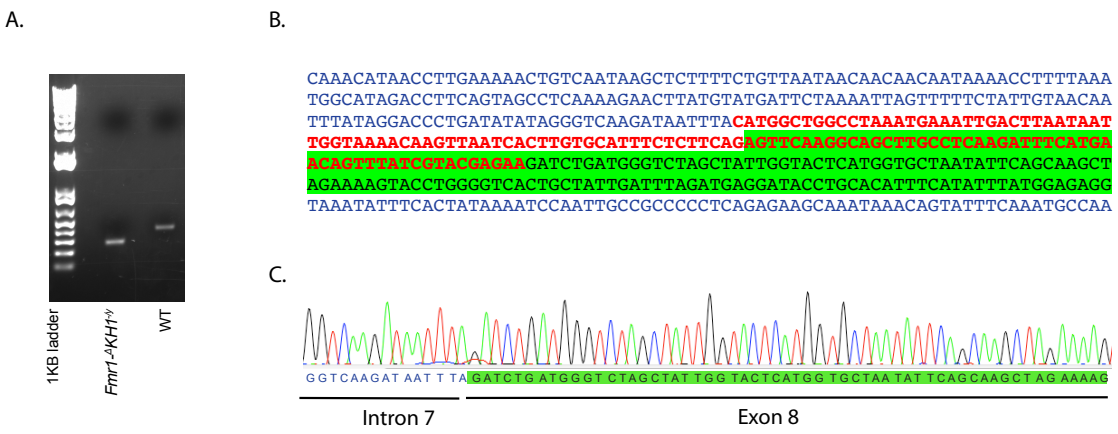

Supplementary Figure 1. Validation of the genomic deletion in the *Fmr1* gene. (A) Amplification product of the *Fmr1* genomic region between exon 7 and 9 of the *Fmr1* gene, primed with the Fmr1-G-F and Fmr1-G-R primers (see Supplementary Table 3. **(B)** Depiction of the deleted sequence within the *Fmr1* gene. Partial sequences of introns 7 and 8 are in blue, genomic sequence encoding for exon 8 is highlighted in green, and the deleted sequence that encompasses parts of intron 7 and exon 8 is bold-red. **(C)** Sanger sequencing of the amplification product from *Fmr1-*$^{\Delta}$*KH1*$^{-/y}$ rats (from A), using the Fmr1-G-F primer.

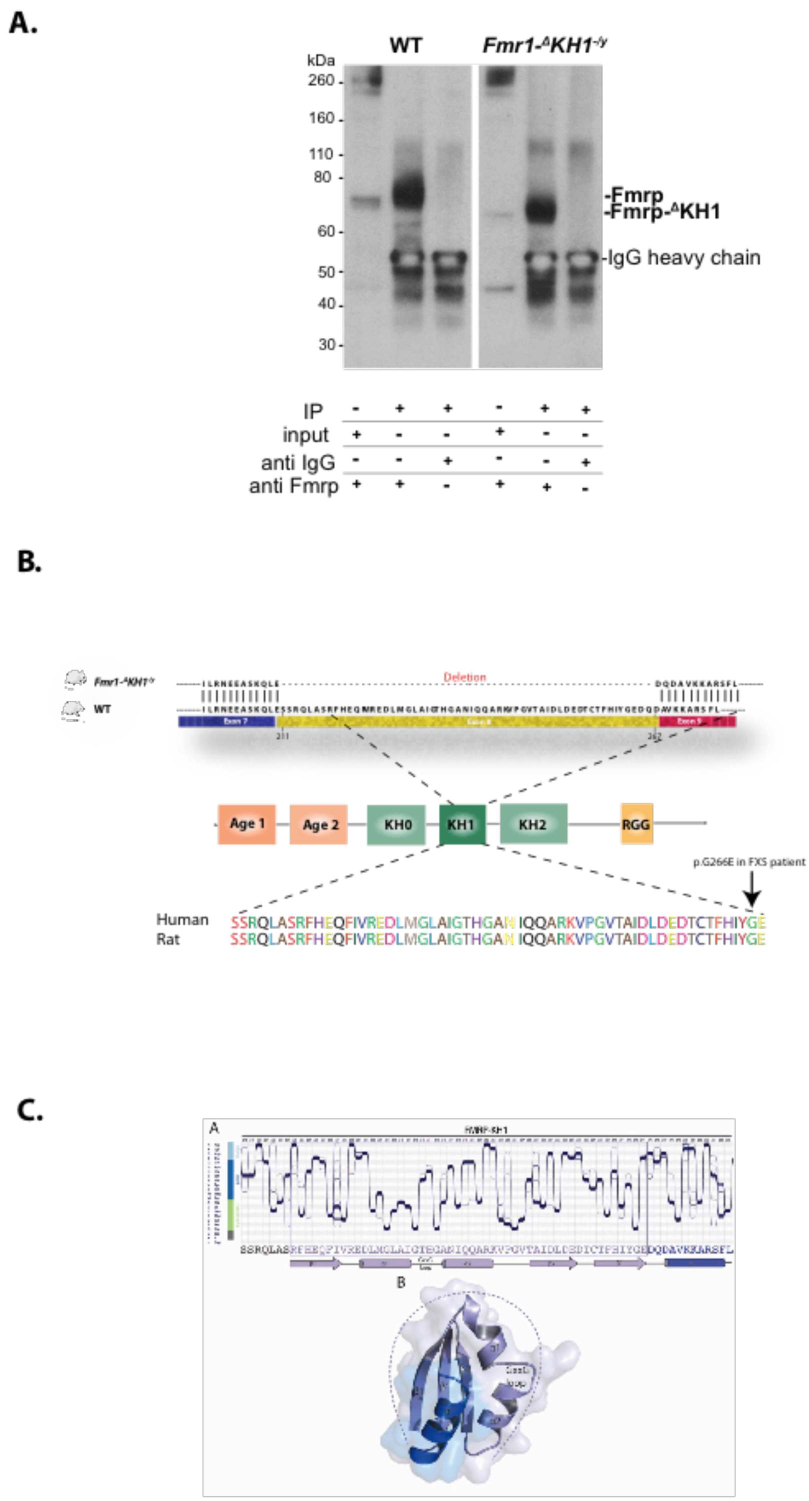

Supplementary Figure 2. The *Fmr1-ΔKH1* rat model lacks the KH1 domain. (A) An IP of Fmrp followed by a immunoblotting with anti-Fmrp antibodies shows a band at the predicted molecular weight of Fmrp (75 kDa) in WT but not *Fmr1-ΔKH1-/y* rats and a new

band at ~70 kDa in *Fmr1-$^{\Delta}$KH1$^{-/y}$* but not WT rats, which is predicted to be Fmrp-$^{\Delta}$KH1. (**B**) (Top) An illustration depicting the amino acids that are a part of the KH1 domain of Fmrp that are deleted from Fmrp in *Fmr1-$^{\Delta}$KH1* rats. (Bottom) The location of a mutation within this domain that was previously reported in a subject with FXS**.** ClustalW alignment indicates that this region is 100% conserved across human and rat between amino acids 211-267 in Fmrp (deleted in the *Fmr1-$^{\Delta}$KH1* rat model). (**C**) Sequence conservation of the KH1 domain across 58 FMRP orthologs. The colour code reflects the chemical and physical properties of the amino acids. The topological organization of the KH1 domain is also shown. The deleted residues and the corresponding secondary structure elements are shown in purple. The lower panel shows the ribbon representation of the human FMRP KH1 domain. The deleted region is indicated by a dashed line and shown in purple.

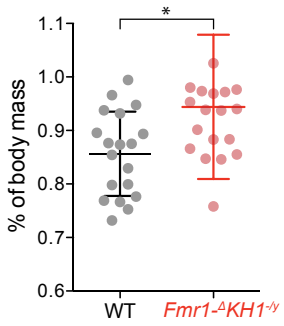

Supplementary Figure 3. Testes:body weight ratio of *Fmr1-$^{\Delta}$KH1$^{-/y}$* rats compared to WT littermates. When controlling for overall body weight, *Fmr1-$^{\Delta}$KH1$^{-/y}$* rats (n=19) have increased testes weight compared to WT littermates (n=19), a hallmark of FXS.

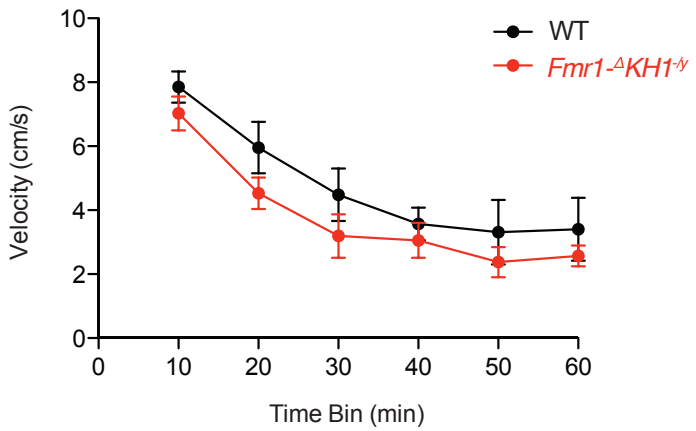

Supplementary Figure 4. Performance of male *Fmr1-$^{\Delta}$KH1$^{-/y}$* rats and WT littermates on the open field test. Male WT, n=6 (black), and *Fmr1-$^{\Delta}$KH1*, n=7 (red) littermates were given one hour to explore a 90 cm x 90 cm open field. Videos were analyzed in 10-minute bins. Both groups decrease in their velocity over time.

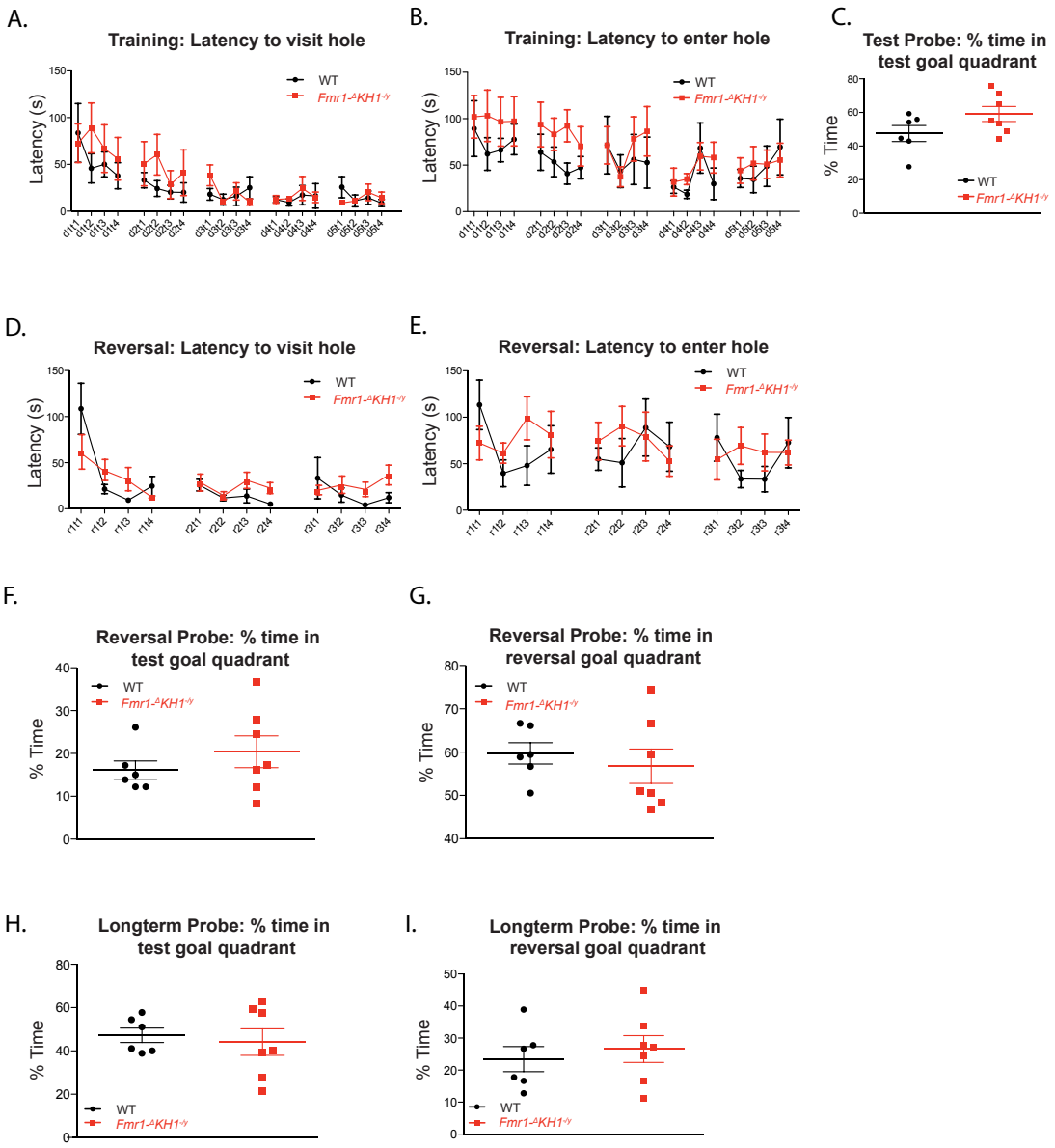

Supplementary Figure 5. Performance of male *Fmr1-$^{\Delta}$KH1$^{-/y}$* rats and WT littermates on the Barnes maze. Male WT, n=6 (black), and *Fmr1-$^{\Delta}$KH1*, n=7 (red), littermates were trained on the Barnes maze to find a target hole with an escape box over four days (training), given a probe test without the escape box, trained to find a hole on the opposite size of the maze (reversal), given another probe test, and, finally, tested two weeks later (long-term probe). (**A**) The time it took for the rat to initially find the hole and (**B**) enter it during the training phase. (**C**) The percentage of time the rat spent in the quadrant of the maze containing the target hole during the probe test. (**D**) The time it took for the rat to initially find the hole and (**E**) enter it during the reversal phase. The percentage of time the rat spent in the quadrant of the maze containing the (**F**) target

hole and (**G**) reversal hole during the reversal probe test. The percentage of time the rat spent in the quadrant of the maze containing the (**H**) target hole and (**I**) reversal hole during the long-term probe test two weeks later.

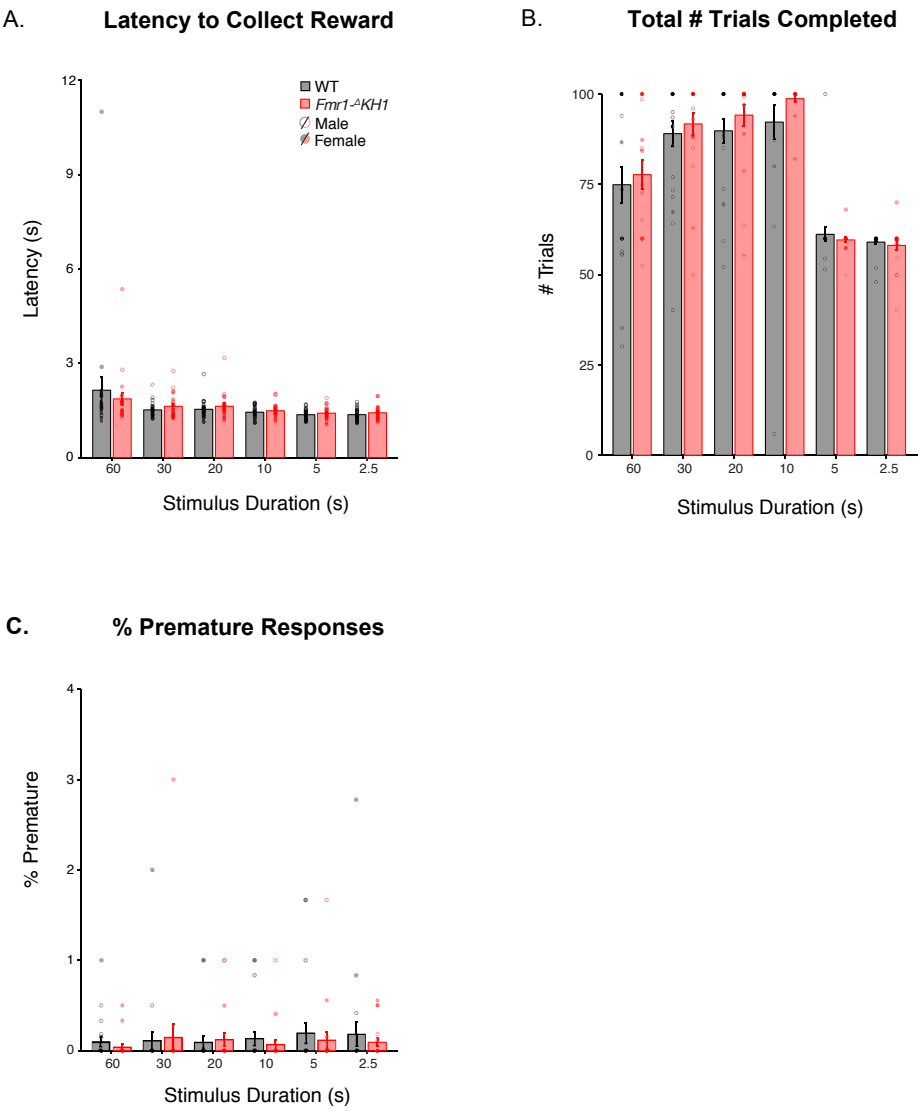

Supplementary Figure 6. Latency to collect reward and premature responses in *Fmr1-$^{\Delta}$KH1* rats and WT littermates on the 5-CSRTT. Across six 5-CSRTT training stages, bars indicate (**A**) mean latency to collect reward ± SEM (WT, n = 22; *Fmr1-$^{\Delta}$KH1*, n = 20), (**B**) mean number of total trials completed each session, and (**C**) mean percentage of premature responses in male and female rats, black = WT, red = *Fmr1-$^{\Delta}$KH1*, open circles = males, filled circles = females, ***$p < 0.001$, **$p < 0.01$, *$p < 0.05$.

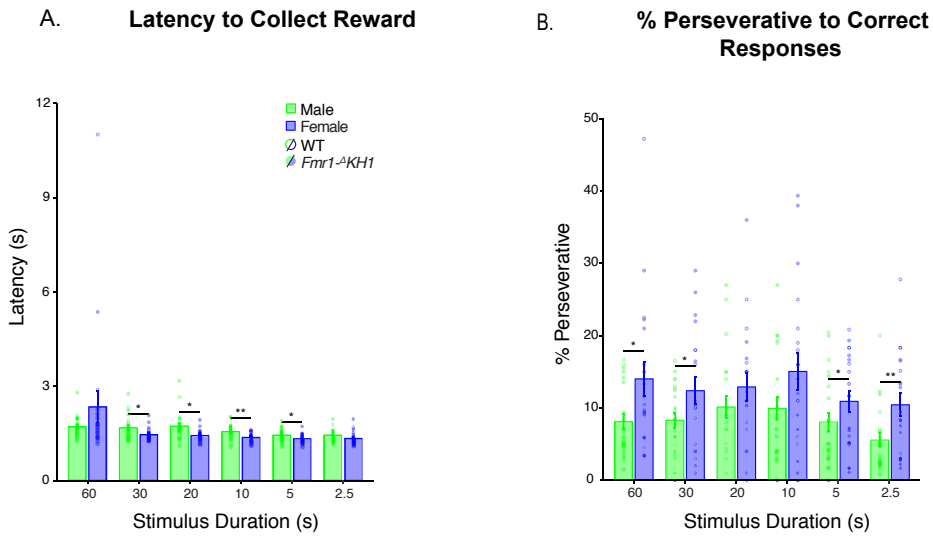

Supplementary Figure 7. Performance of male and female *Fmr1-$^{\Delta}$KH1* rats and WT littermates on the 5-CSRTT. Across six 5-CSRTT training stages, bars indicate (**A**) mean latency to collect reward and (**B**) mean percentage of perseverative responses after a correct choice in males and females ± SEM (males, n = 22; females, n = 32), green = male, blue = female, open circles = WT, filled circles = *Fmr1-$^{\Delta}$KH1*, ***p < 0.001, **p < 0.01, *p < 0.05.

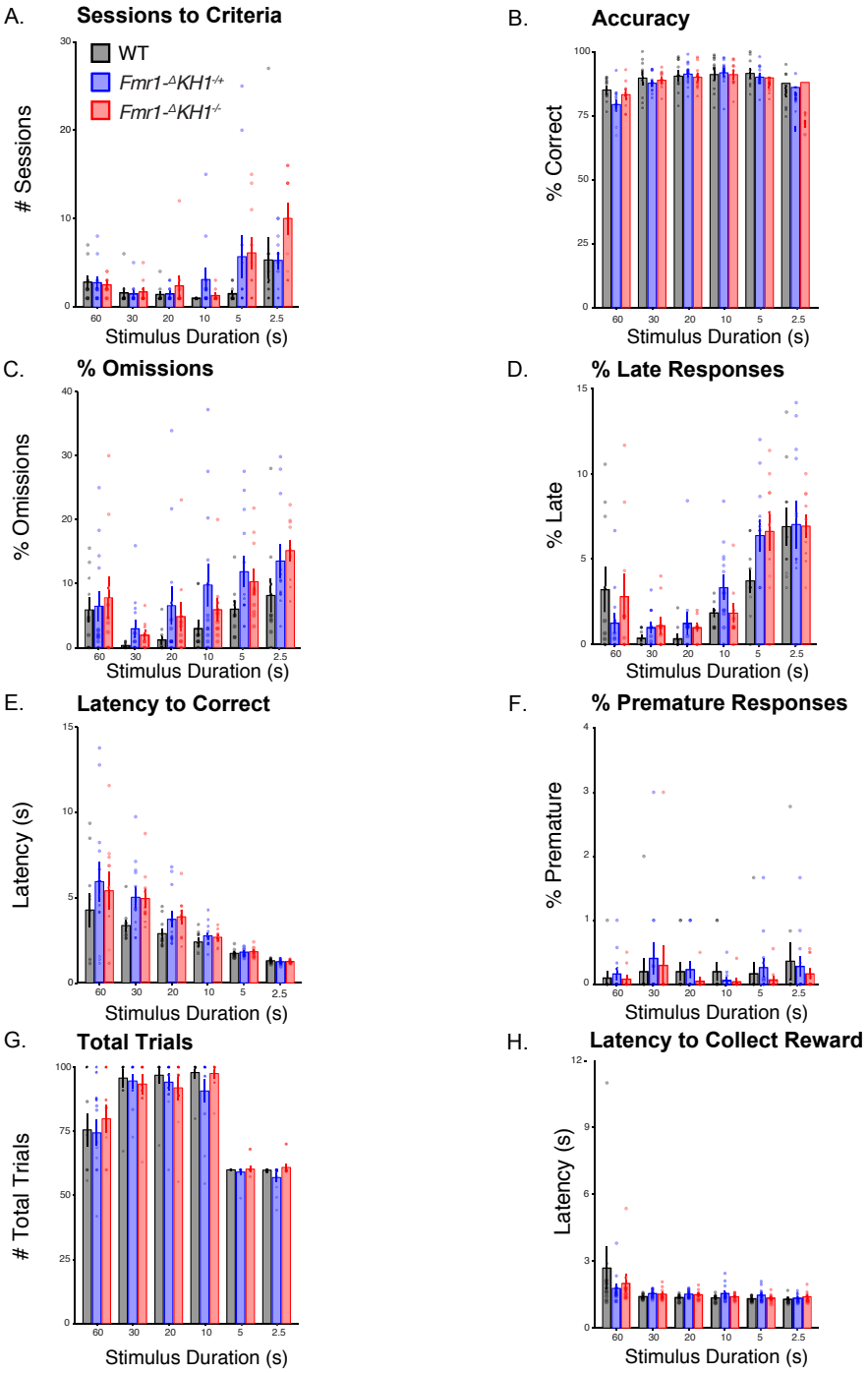

Supplementary Figure 8. Performance of WT, *Fmr1-$^{\Delta}$KH1$^{+/-}$*, and *Fmr1-$^{\Delta}$KH1$^{-/-}$* rats on the 5-CSRTT. (**A**) Across six 5-CSRTT training stages, bars indicate mean number of sessions required to reach criterion ± SEM (WT, n = 10; *Fmr1-$^{\Delta}$KH1$^{+/-}$*, n = 12; *Fmr1-$^{\Delta}$KH1$^{-/-}$*, n = 10), (**B**) mean accuracy (# correct / # total responses), (**C**) mean percentage of trials that were omitted, (**D**) mean percentage of trials with a late response, (**E**) mean latency to perform a correct response, (**F**) mean percentage of trials with a premature

response, (**G**) mean number of total trials completed each session, and (**H**) mean latency to collect a reward, black = WT, blue = *Fmr1-$^{\Delta}$KH1$^{+/-}$*, red = *Fmr1-$^{\Delta}$KH1$^{-/-}$*, ***p < 0.001, **p < 0.01, *p < 0.05.

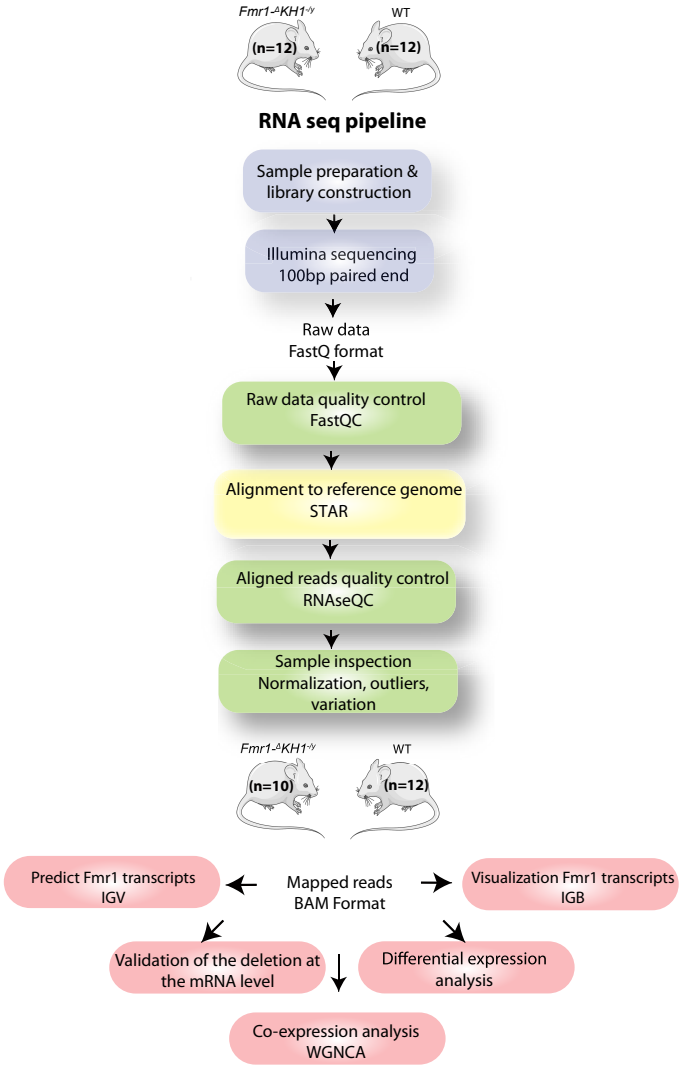

Supplementary Figure 9. RNAseq analysis pipeline. An illustration of the pipeline applied for RNAseq analysis starting with library preparation, sequencing, quality control steps to inspect both, the raw data and the aligned reads, alignment to reference genome, normalization and outlier inspection, validation of the deletion, and finally differential gene expression and co-expression analysis (see the Methods section for details).

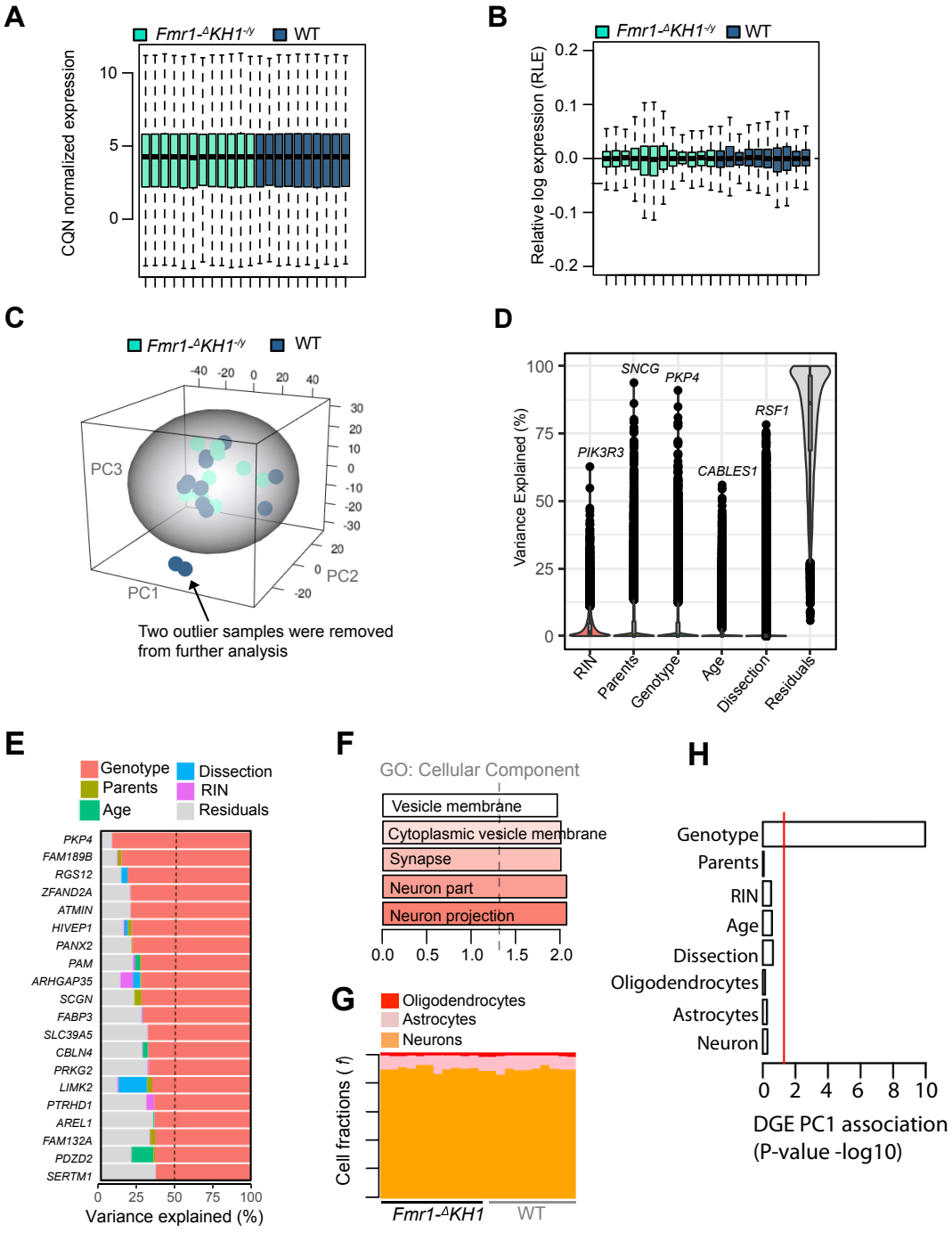

Supplementary Figure 10. RNA-seq quality control and data pre-processing. (A) Conditional quantile normalization (CQN) boxplots and **(B)** relative log expression (RLE) gene expression across *Fmr1-ΔKH1* and WT rats. **(C)** Principal component analysis (PCA) of CQN normalized expression data with an ellipse fit two standard deviations from the grand mean. **(D)** variancePartition analysis of global gene expression profiles

identifies genes with variance is explained by RIN, parents, genotype (*Fmr1-$^{\Delta}$KH1* and WT) age and dissection date. **(E)** The top 20 genes who variance (>50%) is explained by differences in genotype and **(F)** their functional annotation. **(G)** Cibersort cell type deconvolution analysis of global expression profiles across *Fmr1-$^{\Delta}$KH1$^{-/y}$* and WT samples. **(H)** PCA was applied using all genes with DGE signatures passing FDR $P < 0.1$. The resulting PC1 was associated with measurable factors, including genotype, parents, RIN, age, date of dissection and estimated cell type frequencies. PC1 was predominately associated with differences in genotype and not with any other factors.

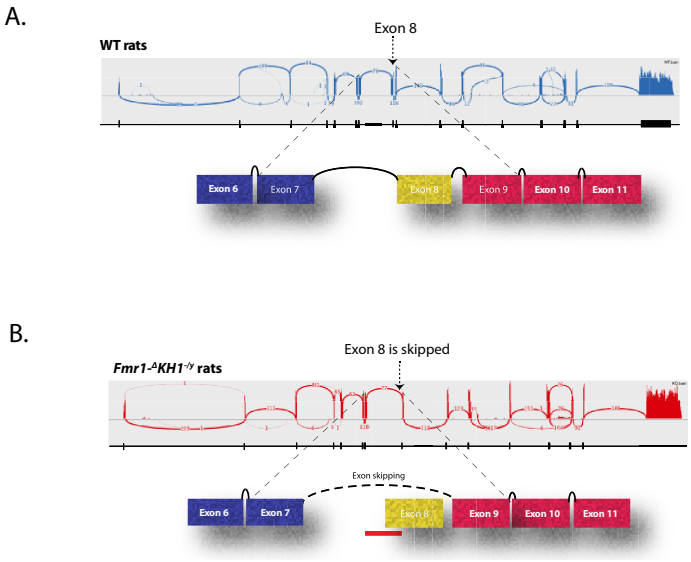

Supplementary Figure 11. Skipping of Exon 8 of *Fmr1* mRNA based on RNAseq data. (A) Top: Sashimi plots for WT samples created using RNAseq show the coverage for each alignment track plotted as a bar graph. Arcs display splice junctions that connect exons and contain the number of reads split across the junction (junction depth). Genomic coordinates and the gene annotation track are shown below the junction tracks. Bottom: An illustration that shows that exon 8 is read in WT rats. **(B)** Top: Sashimi plots for *Fmr1-$^{\Delta}$KH1$^{-/y}$* samples. Bottom: An illustration that shows that the sequence of exon 8 is skipped, but exon 7 and 9 are in frame in *Fmr1-$^{\Delta}$KH1$^{-/y}$* rats.

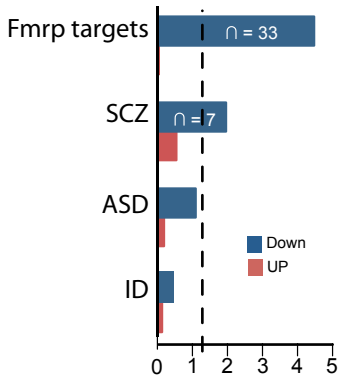

Supplementary Figure 12. Enrichment of differential gene expression signatures. Down-regulated *Fmr1-$^{\Delta}$KH1$^{-/y}$* DGE signatures are enriched for Fmrp targets and SCZ genetic risk loci.

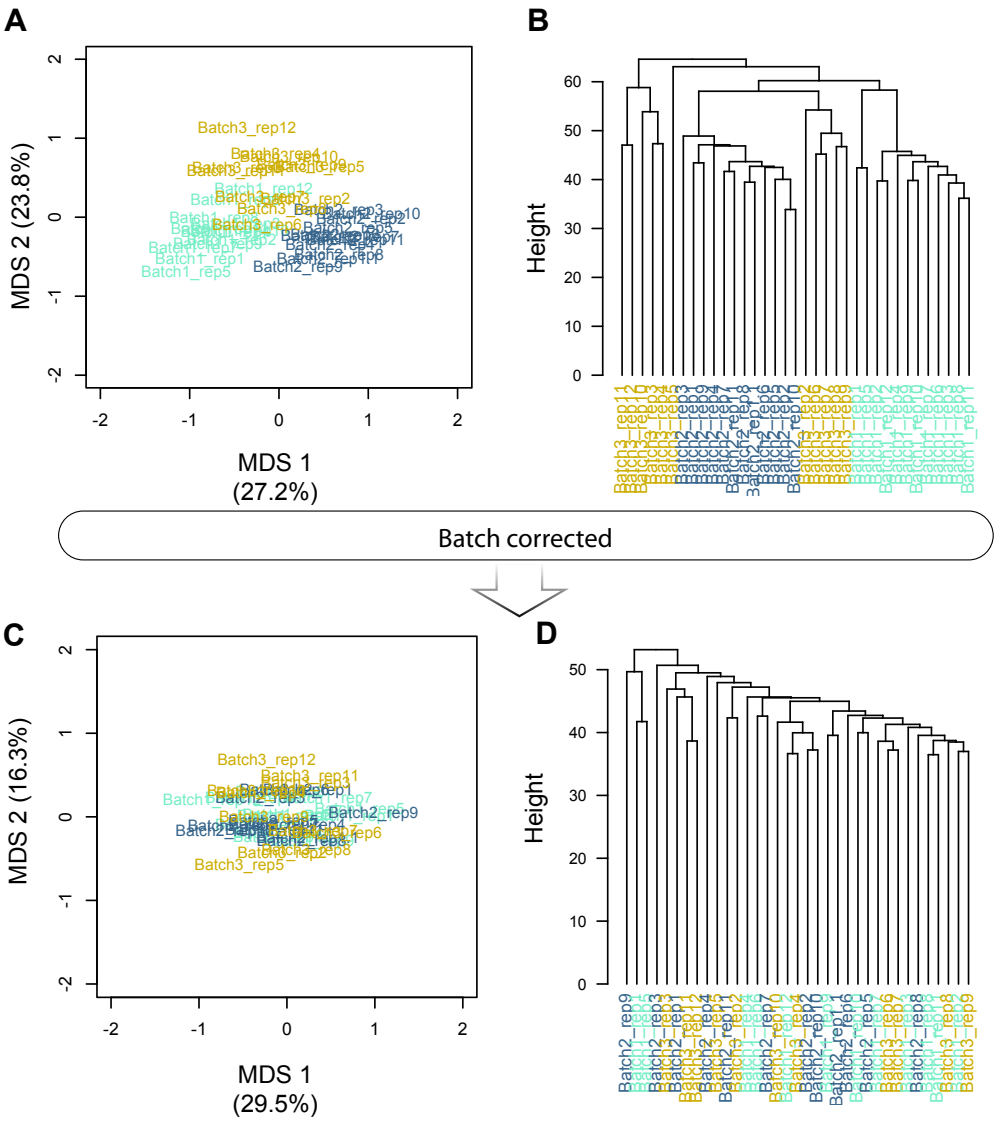

Supplementary Figure 13. Batch correction for RNA-sequencing data of mPFC from three independent batches of WT rats. **(A)** Multi-dimensional scaling (MDS) and **(B)** unsupervised hierarchical clustering (Euclidian distance and ward's clustering) revealing a substantial fraction of variability in gene expression explained by batch effects. **(C)** MDS and **(D)** unsupervised clustering following combat correction, indicating reduced batch effects by processing date.